Cosmogenic nuclide chronology of millennial-scale glacial advances during O-isotope stage 2 in Patagonia

Michael R. Kaplan†
Department of Geology and Geophysics, University of Wisconsin, Madison, Wisconsin 53706, USA

Robert P. Ackert, Jr.
Department of Marine Chemistry and Geochemistry, Woods Hole Oceanographic Institution, Clark 419, MS 25, Woods Hole, Massachusetts 02543, USA

Brad S. Singer
Daniel C. Douglass
Department of Geology and Geophysics, University of Wisconsin, Madison, Wisconsin 53706, USA

Mark D. Kurz
Department of Marine Chemistry and Geochemistry, Woods Hole Oceanographic Institution, Clark 419, MS 25, Woods Hole, Massachusetts 02543, USA

ABSTRACT

The terrestrial glacial record reflects past snowline variability and atmospheric temperature changes. When combined with secure chronologies, these data can be used to test models of ice-age climate. We present new in situ cosmogenic ^{10}Be, ^{26}Al, and ^{3}He exposure ages, supported by limiting ^{40}Ar/^{39}Ar and ^{14}C ages, for seven of the youngest moraines east of Lago Buenos Aires, Argentina, 46.5°S, that were deposited by a large outlet glacier of the Patagonian Ice Cap. Following a major glaciation that deposited extensive moraines prior to 109 ka, paired ^{10}Be-^{26}Al ages indicate that the next youngest complex of moraines was deposited from 23.0 ± 1.2 to 15.6 ± 1.1 ka (1σ). During the last glaciation, ice was at its maximum extent prior to 22 ka and at least five moraines were deposited in less than 10 k.y. These data are in good agreement with three ^{14}C ages of ca. 16 ka from varved sediment banked on top of the youngest of these five moraines and limiting ^{3}He ages, which range from ca. 33 to 19 ka. The most extensive ice marginal deposits preserved within the last 109 k.y. were formed during marine oxygen isotope stage 2; no moraines dating to stage 4 were found. For stage 2, the distribution of ages at Lago Buenos Aires is similar to cosmogenic nuclide-based glacial chronologies from western North America. In fact, the structure of the last mid-latitude South American ice age—specifically, the overall timing, a maximum ice extent prior to 22 ka, and deglaciation after 16 ka—is indistinguishable from that of the last major glaciation in the Northern Hemisphere, despite a maximum in Southern Hemisphere insolation during this period. The similar mid-latitude glacial history in both hemispheres implies that a global climate forcing mechanism, such as atmospheric cooling, as opposed to oceanic redistribution of heat, synchronizes the ice age climate on orbital time scales.

Keywords: South America, ice ages, glacial maximum, last, exposure age, paleoclimatology, and geochronology.

INTRODUCTION

A fundamental question in global climate dynamics is whether Southern Hemisphere glaciers respond in step with fluctuations of the Northern Hemisphere ice sheets and mountain glaciers despite antiphased solar insolation. The answer to this question, which remains poorly understood at both low-frequency orbital and high-frequency sub-orbital time scales, has profound implications for understanding the extreme climatic state of the ice-age world. Comparisons of well-dated Southern and Northern Hemisphere glacial chronologies can be used to evaluate whether ice-age climates were anti-phased (Blunier et al., 1998) or uniform (Steig et al., 1998; Denton, 1999) and to determine the relative roles of astronomic, atmospheric cooling, ocean-heat transfer, and ice sheet–sea level forcings (e.g., Denton, 1999; Cane and Clement, 1999; Stocker, 2000). For example, it has been documented that Antarctic ice sheet behavior has broadly followed the 100 k.y. Northern Hemisphere orbital periodicity that characterizes the mid- to late Pleistocene ice age (Broecker and Denton, 1989). However, chronological constraints on lower latitude Southern Hemisphere mountain glacial records are critical for evaluating whether the Northern Hemisphere ice sheets synchronize ice sheet response in Antarctica mainly through sea level changes, or alternatively, whether a global climate forcing such as atmospheric temperature is also pertinent (Denton, 1999).

High-resolution dating of terrestrial glacial records from southern South America thus provides a key to unraveling the processes that drive glacial climates. The terrestrial glacial record adjacent to Lago Buenos Aires, Argentina (Fig. 1), 46.5°S, comprises one the world's most complete and intact sequences of Quaternary moraines (Rabassa and Clapperton, 1990). In a companion paper, Singer et al.

†Present address: School of GeoSciences, University of Edinburgh, Drummond Street, Edinburgh EH8 9XP, Scotland, UK; e-mail: mkaplan@geo.ed.ac.uk.

GSA Bulletin; March/April 2004; v. 116; no. 3/4; p. 308–321; doi: 10.1130/B25178.1; 5 figures; 5 tables.

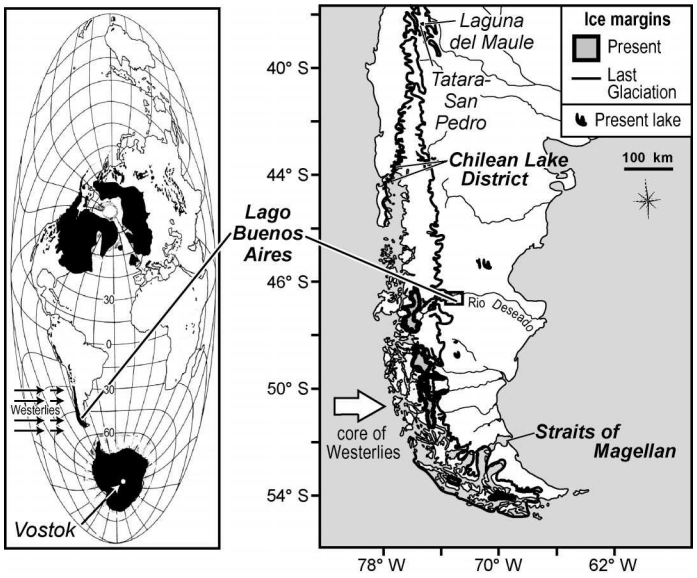

Figure 1. Location of Lago Buenos Aires moraine sequence. Left map highlights location within Americas, present latitudinal range of Southern Hemisphere Westerlies, and hypothesized glacial coverage during marine isotope stage 2 in black (Denton and Hughes, 1981). Right map highlights place names, present approximate latitude of core of Southern Hemisphere Westerlies, and glacial extent during last ice age as originally mapped by monumental work of Caldenius (1932).

(2004) describe the geologic setting and stratigraphic relations between the glacial deposits and $^{40}Ar/^{39}Ar$ and K-Ar dated basalt flows, which demonstrate that these deposits span the last 1 m.y. This paper presents the results from two independent chronometers, specifically, in situ cosmogenic (^{10}Be-^{26}Al-^{3}He) surface exposure dating of moraine boulders and ^{14}C dating of glacial-lacustrine sediment that constrains the age of the youngest moraines. The inferences and conclusions are strengthened by the general agreement of the multi-isotope data sets.

These data represent some of the first surface exposure ages of moraines in mid-latitude South America that proxy for the past oscillations of the Andean snowline and paleoclimate. The new chronology from 46° S supports the hypothesis that the mid-latitudes of both hemispheres witnessed a strikingly similar glaciation during marine oxygen isotope stage 2. The new chronology from Lago Buenos Aires can be compared to ^{14}C-dated records elsewhere in South America such as in the Lake District and Straits of Magellan and glacial records from Antarctica and the Northern Hemisphere (Fig. 1). At Lago Buenos Aires, and along more than 1300 km of the southernmost Andes, exposure dating is ideally suited for resolving the age of individual moraines and glacial periods. South of the Chilean Lake District (Fig. 1), on the west side of the Andes, the Patagonian ice cap calved into the Pacific Ocean, and terminal ice margin deposits are lacking (Mercer, 1983). To the east, on the dry steppes in the rain shadow of the Andes, the use of ^{14}C is limited by the sparseness of preserved organic material and the age of the deposits; most glacial deposits east of the southern Andes predate the last glaciation and the ~40 k.y. limit of ^{14}C dating (this study; Mercer, 1969, 1976, 1983; Mörner and Sylwan, 1989; Rabassa and Clapperton, 1990; Ton-That et al., 1999; Singer et al., 2004).

GEOLOGIC SETTING

Singer et al. (2004) describe the Lago Buenos Aires area and >1 m.y. glacial sequence in detail. Here we briefly review aspects of the record that are essential for understanding the results and conclusion of this paper. Surficial geologic mapping has delineated evidence of at least 19 moraines and associated outwash plains deposited east of Lago Buenos Aires (Figs. 2 and 3). Following Caldenius (1932), the moraines have been grouped into four broadly defined moraine complexes that we informally named Fenix, Moreno, Deseado, and Telken. The $^{40}Ar/^{39}Ar$ and K-Ar chronology (Singer et al., 2004) indicate that the Telken VI–I moraines were deposited between 1016 and 760 ka, the Deseado and Moreno moraines between 760 and 109 ka, and the Fenix moraines after 109 ka. Here, we use in situ cosmogenic ^{10}Be, ^{26}Al, and ^{3}He to place temporal constraints on the individual Fenix and Moreno I moraines (Figs. 2 and 4), which record at least two major glaciations.

The Moreno I moraine tops a prominent west-facing escarpment (Figs. 2 and 3) ~20 km east of the lake (Fig. 2). Outwash graded to the Moreno I moraine forms a discontinuous terrace at ~460–440 m above sea level (asl) along the south side of the Rio Deseado valley (Fig. 2). This terrace is buried by the Cerro Volcán basalt flow (Fig. 2; also see Fig. 4C *in* Singer et al., 2004). Moreno boulders commonly exhibit ventification, but boulder spallation or exfoliation are relatively uncommon.

The Fenix moraines are generally sharp-crested ridges that lie at 450–480 m asl. They are 10–30 m high and up to 500 m wide (Figs. 2 and 3, A and B). The individual moraine ridges are relatively continuous and they can be easily traced around the Lago Buenos Aires Valley, except for Fenix III, which consists of only a few isolated crests surrounded by younger outwash (Fig. 2). Spectacular sized, subrounded blocks up to 20 m high (Fig. 3, C and F) of columnar jointed basalt with striations and glacial polish stand along the crests of the Fenix I and II moraines. Large basaltic blocks also occur on the other moraines, but they are much less abundant and smaller. Erratic cobbles and boulders of granite, rhyolite, diorite, gneiss, schist, and other lithologies clearly derived from the Andean Cordillera >50 km to the west are commonly found on all Lago Buenos Aires moraines (Singer et al., 2004). Spallation is rarely observed on Fenix moraine boulders.

The Menucos moraine is grouped within the Fenix moraine system (Singer et al., 2004), and it is the youngest ice margin position delineated at the eastern end of Lago Buenos Aires; in the field area, it is a topographically minor ridge (Fig. 2) containing large blocks of basalt up to 20 m in diameter. The Menucos moraine was deposited on top of ~887 measured varves that decrease in thickness upward (Caldenius, 1932; Sylwan, 1989) and are exposed along the Rio Fenix Chico (Fig. 2). The varved sediments are banked upon, and therefore they are younger than, the Fenix I moraine (Caldenius, 1932; Singer et al., 2004).

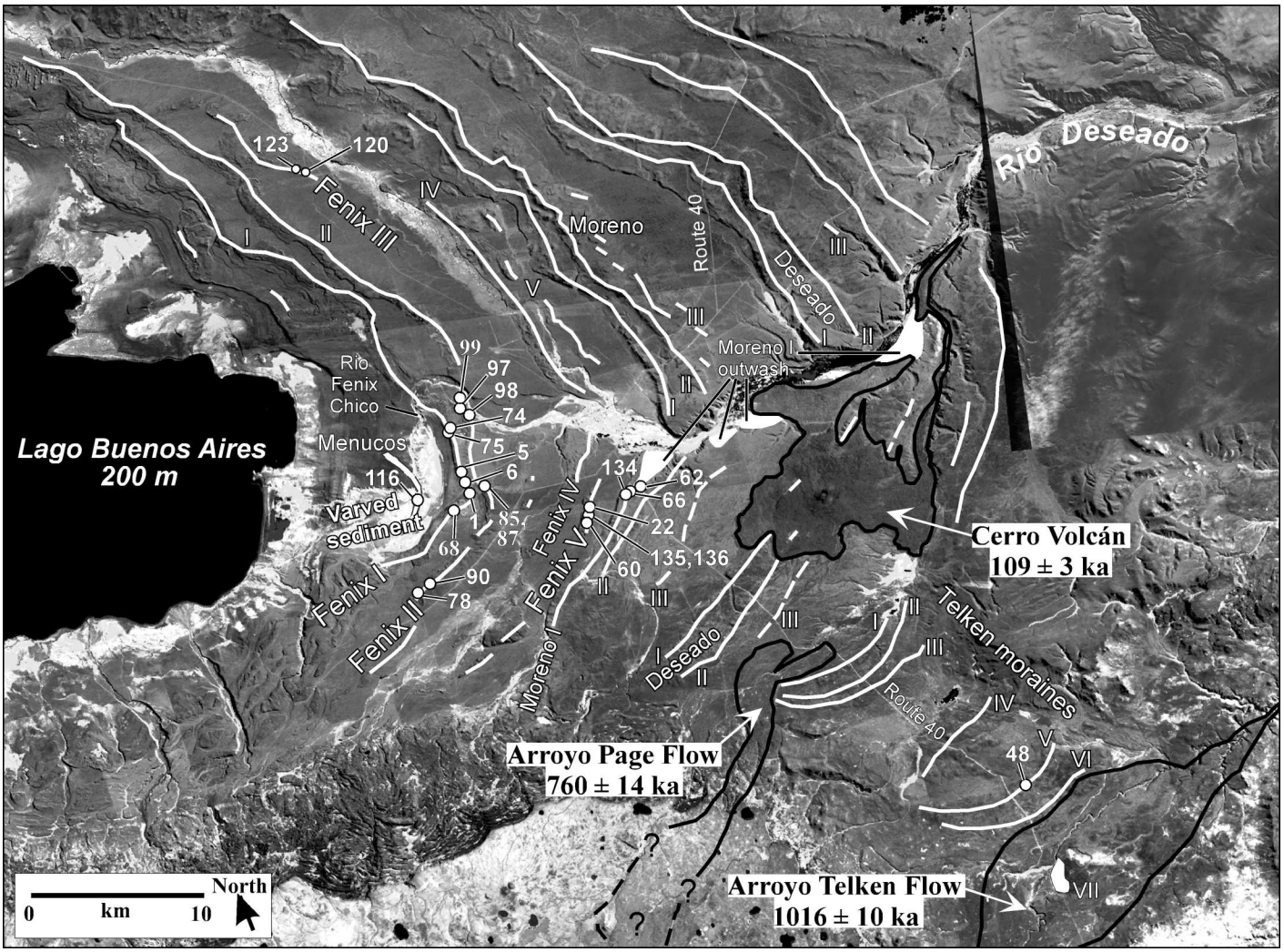

Figure 2. Landsat image showing youngest moraines around eastern end of Lago Buenos Aires, lava flows (ages ± 2σ), locations of measured samples, and area of varved section (See Singer et al., 2004).

GEOCHRONOLOGY METHODS

Radiocarbon Dating

Material dateable with ^{14}C has been found only at one site, in the varved section exposed by the Rio Fenix Chico (Fig. 2). Approximately 1 kg of carbonate-cemented concretions from a varve within the lower third of the sediment section yielded 1 mg of pure C in the University of Zurich ^{14}C laboratory. Previously, Sylwan (1989) obtained two ^{14}C ages on carbonate-cemented concretions from the same varved outcrop (Table 1). Sylwan's (1989) samples were separated by ~280 varve couplets.

Cosmogenic Surface Exposure Dating

Sample Collection and Preparation

Given the excellent preservation of the moraine record and the lack of associated organic material due to the arid climate, cosmogenic dating is ideally suited for dating individual moraines at Lago Buenos Aires. Excellent summaries of the principles of cosmogenic nuclide dating include Lal (1991), Cerling and Craig (1994), Kurz and Brook (1994), and Gosse and Phillips (2001). Here we only briefly review sampling procedures, principles, methodologies, and systematic corrections that are particularly relevant for understanding the application of this technique in the region of Lago Buenos Aires.

The geomorphic setting and surficial characteristics were considered carefully when choosing boulders to sample. For example, we avoided boulders with evidence of rock splitting or spallation. Instead, we sampled boulders that appear to have been eroding only by granular disintegration. We also avoided edges and sharp facets by sampling at least 5 cm from these features. Except for shielded material, sampling was close to the center of top surfaces of boulders that dip less than 15° and usually less than 10°. Samples were collected from the upper few centimeters of moraine boulders with hammer and chisel. We generally selected the largest boulders available (Table 2), on, or nearly on, well-defined moraine crests (Fig. 3) that are likely to have been stable and to have stood above deposited snow or volcanic ash. We aimed for boulders at least 1 m high and wide, but the full range in height varied from ~25 m to 32 cm for Fenix samples (Table 2), with basaltic boulders on Fenix II being the tallest (Fig. 3, C and F). On the part of Moreno I sampled (Fig. 2), well-defined continuous crests were lacking and boulders were rare. Thus, the two samples LBA-01–62 and 66 are not ideal, standing only ~25 cm and 5 cm high. Sample

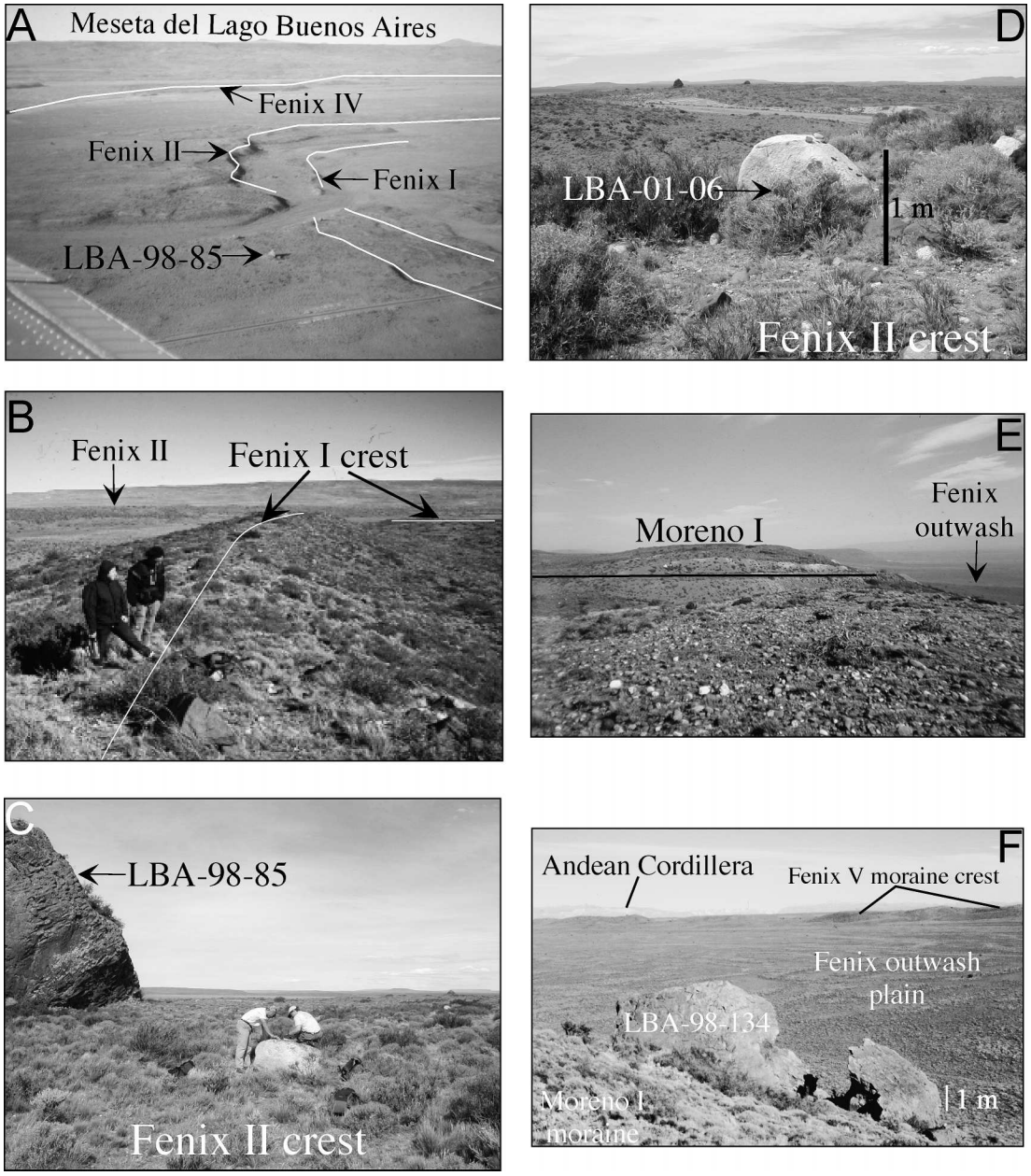

Figure 3. Photographs of Fenix and Moreno I moraines. (A) Looking south, aerial view of Fenix moraines, with crests marked white. The 14-m-high basaltic boulder on Fenix II moraine is sample LBA-98–085. Lago Buenos Aires is ~10 km to right. (B) Looking north along Fenix I moraine crest, marked by white line. (C) On Fenix II moraine, 14-m-tall basaltic boulder on left is sample site LBA-98–085 (see A above). Sampling granitic boulder on right. (D) Sample LBA-01–06 on Fenix II moraine. (E) Looking south, on north side of study area (Fig. 2) on Moreno I crest. For scale, Route 40 is black line toward background. Also note that on right is Moreno scarp separating Moreno from lower Fenix systems. (F) Looking northwest, ^{3}He sample LBA-98–134 on Moreno I.

LBA-01–66 can be actually considered a large ''clast,'' ~16 × 19 cm, which was sitting entirely on top of the surface. All elevations were measured relative to a 591 m benchmark using a barometric-based altimeter (analytical precision ± 0.1 m) that was cross-checked with global positioning system (GPS) and topographic maps. Based on comparison between GPS and barometric-based altimeter measurements, elevation accuracy is estimated to be 10–20 m.

Although we have attempted to minimize geologic uncertainties by sampling strategies discussed above, some scatter in the data may be attributed to geologic factors such as prior exposure, variable erosion rates, postdepositional movement, and burial and exhumation. Snow cover is not corrected for, but it is assumed to be insignificant (< 1%) because we sampled along tops of moraine crests and, at present, total annual precipitation is less than ~250 mm and appreciable accumulation usually lasts less than a month. Whereas these processes should have had a small or negligible effect on the exposure ages from the Fenix moraines (i.e., below analytical uncertainty) because they are relatively young, they

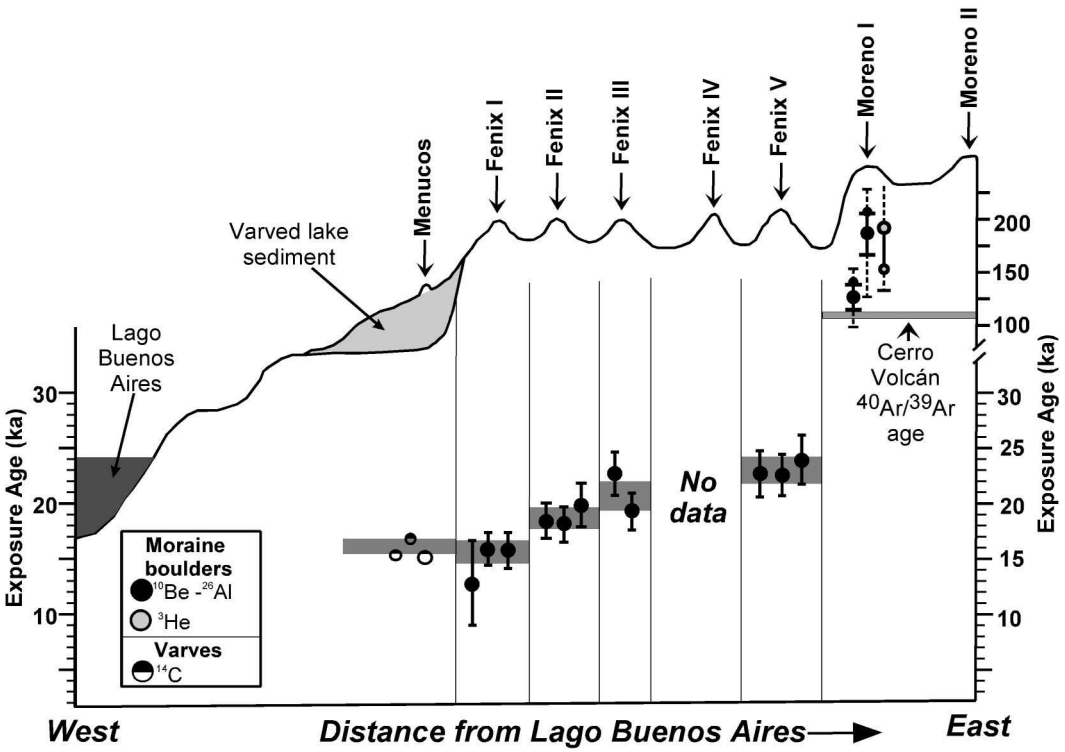

Figure 4. Schematic topographic profile from Lago Buenos Aires to Moreno II with chronology for moraines and varved section. Also shown is 109 ± 3 (2σ) ka Cerro Volcán flow (Fig. 2) stratigraphically underlying Moreno complex. Vertical range of, and horizontal line within, each ^{14}C symbol indicate calibrated solution range and mean age, respectively (Table 1); horizontal gray band for varved section reflects uppermost and lowermost bounds of all calibrated solution ranges. For each Fenix moraine, boulder ^{10}Be-^{26}Al ages shown include all propagated errors except that for production rate (see text). Shaded band for each moraine represents its weighted mean age ± 1σ (Table 5). For Moreno ^{10}Be-^{26}Al ages (Table 2), lowest error bar represents 1σ minimum age with zero erosion and local production rates; lower filled circle is mean age with 2.3 mm/k.y. erosion rate and local production rates, with associated errors represented by wide error bars; upper circle is mean age with Stone (2000) production rates and erosion; highest error bar represents maximum 1σ age with Stone production rates and erosion. For Moreno ^{3}He age (Table 4), lower error bar is shielded, corrected age with zero erosion rate; lower circle is age without shielding correction and no erosion; upper circle is shielded, corrected age with 2.3 mm/k.y. erosion rate; uppermost dashed line points toward age with global production rate (Licciardi et al., 1999).

TABLE 1. ^{14}C DATA ON VARVED SECTION, LAGO BUENOS AIRES

Sample†	^{14}C age (^{14}C yr B.P. ± 1σ)	$\delta^{13}C$ (‰)	Calibrated age (solution range) (cal yr B.P.) (±1σ)‡	Reference
St 10005§	14065 ± 345	NA	16864 (17332–16409)	Sylwan (1989)
St 10503§	12840 ± 130	NA	15476 (15709–14590)	Sylwan (1989)
UZ-3921/ETH-15654	12880 ± 160	–21.8	15512 (15779–14923)	This study

Note: NA—data not archived.

†St—Laboratory of Isotope Geology, National Museum of Natural History at Stockholm; UZ—University of Zurich; ETH—Swiss Federal Institute of Technology.

‡Calibrated according to Stuiver et al. (1998).

§If varves are annual (Sylwan, 1989), then sample St 10005 is separated by sample St 10503 by about 280 yr of deposition.

might significantly impact the ages from the older moraines given their cumulative effect over a long time (Lal, 1991), especially for small samples such as LBA-01–66.

For ^{10}Be and ^{26}Al dating, the selected boulders were granitic rocks except for LBA-01–05 (quartz pebble conglomerate), LBA-01–62 and 66 (quartz veins in metamorphic rocks), and LBA-01–48 and LBA-98–123 (red and gray rhyolites, respectively). Glacial striations were not observed and boulder surface microrelief is typically about or less than 1 cm. Quartz was separated and purified from other minerals at the University of Wisconsin using standard methods of crushing, sieving, heavy liquids, and repeated acid leaching. Subsequently, ion-exchange chromatography and precipitation techniques chemically isolated Be and Al (Kohl and Nishiizumi, 1992). Stable Al was measured by inductively coupled plasma atomic emission spectroscopy (ICP-AES) at the University of Colorado at Boulder. $^{10}Be/^{9}Be$ and $^{27}Al/^{26}Al$ isotope ratios were measured at the Center of Accelerator Mass Spectrometry at Lawrence Livermore National Laboratory and compared to procedural blanks (Table 2) and their laboratory standards.

Samples for ^{3}He measurements were collected from three lithologies of basalt boulders, as shown by major element analyses (Table 3; Ton-That et al., 1999) that confirmed original identification based on hand specimens and boulder morphology. Six of the nine samples appear to be the same lithology, a fine-grained basalt with rare, small lherzolite xenoliths up to 4 mm in diameter. Olivine

TABLE 2. ^{10}Be AND ^{26}Al DATA FROM MORAINE BOULDERS AT LAGO BUENOS AIRES, 46.5°S

Sample	Elev. (m)	Height (cm)	Lat. (°S)	Long. (°W)	^{10}Be (10^5 atoms gm^{-1} ± 1σ)	^{26}Al	Age 1 (ka)†				Age 2 (ka)†						Boulder age§			
							^{10}Be	±1σ#	^{26}Al	±1σ#	^{10}Be	±1σ#	±1σ††	^{26}Al	±1σ#	±1σ††	ka	±1σ††	ka	±1σ‡‡
Fenix I moraine																				
LBA-01-01	445	~115	46° 36′ 14.2″	71° 02′ 08.7″	no data	6.091 ± 1.583	no data		12.5	3.3	no data			12.8	3.4	3.9	12.8	3.9	12.8	3.9
LBA-01-05	438	25–30	46° 35′ 43.2″	71° 02′ 15.3″	1.194 ± 0.038	10.093 ± 2.217	15.0	0.5	21.0	4.7	15.5	0.5	1.6	21.9	4.9	5.9	15.9	1.5	16.0	1.6
LBA-01-06	438	~100	46° 35′ 37.0″	71° 56′ 11.0″	1.395 ± 0.110	6.201 ± 0.690	17.6	1.4	12.8	1.5	18.2	1.4	2.3	13.2	1.6	2.4	15.8	1.6	15.8	1.7
Fenix II moraine																				
LBA-98-78	454		46° 37′ 35.2″	71° 02′ 34.9″	1.374 ± 0.049	9.689 ± 0.597	17.1	0.6	19.8	1.5	17.7	0.6	1.8	20.6	1.5	3.2	18.4	1.6	18.4	1.6
LBA-98-97	430	85.0	46° 33′ 20.3″	71° 01′ 35.3″	1.381 ± 0.051	8.276 ± 1.207	17.5	0.6	17.3	2.6	18.2	0.6	1.9	17.9	2.7	3.7	18.1	1.7	18.1	1.7
LBA-98-98	430	57.0	46° 33′ 20.3″	71° 01′ 35.3″	1.502 ± 0.048	6.197 ± 0.620	19.1	0.6	12.9	1.4	19.9	0.6	2.0	13.3	1.4	2.3	19.9	2.0	19.9	2.1
Fenix III moraine																				
LBA-98-120	510	75.0	46° 24′ 18.8″	71° 04′ 20.1″	1.754 ± 0.066	10.331 ± 0.867	20.6	0.8	25.8	2.0	21.5	0.8	2.2	27.2	2.1	4.3	22.8	2.0	22.9	2.3
LBA-98-123	510	80.0	46° 24′ 17.4″	71° 04′ 24.5″	1.700 ± 0.052	8.394 ± 0.627	19.9	0.6	16.2	1.4	20.8	0.6	2.1	16.7	1.4	2.7	19.3	1.6	19.1	1.9
Fenix V moraine																				
LBA-98-135	439	80.0	46° 37′ 22.6″	70° 57′ 27.0″	1.748 ± 0.052	10.287 ± 2.066	21.7	0.6	21.1	4.3	22.8	0.7	2.3	22.0	4.5	4.3	22.7	2.1	22.7	2.4
LBA-01-22	452	32.0	46° 37′ 16.6″	70° 57′ 11.7″	1.762 ± 0.045	10.038 ± 0.507	21.8	0.6	21.1	1.3	22.8	0.6	2.3	22.1	1.4	2.7	22.6	1.9	22.6	2.1
LBA-01-60	439	~75	46° 37′ 23.7″	70° 57′ 30.7″	1.922 ± 0.067	9.687 ± 1.137	24.0	0.8	19.9	2.5	25.3	0.9	2.6	20.8	2.6	5.6	23.9	2.2	23.7	2.4
Moreno moraine																				
LBA-01-62	475	18-20	46° 37′ 27.9″	70° 54′ 32.5″	9.556 ± 0.219	50.003 ± 1.559	144.7	3.3	141.2	6.6	210.9	4.9	27.3	198.4	9.3	36.1	206.4	21.8	206.3	22.1
LBA-01-66	457	3-5	46° 37′ 57.0″	70° 55′ 29.4″	11.750 ± 0.271	67.577 ± 1.641	115.0	2.6	100.9	5.1	151.3	3.5	17.7	125.2	6.4	20.5	140.1	13.4	140.0	13.6
LBA-01-62§§					Calculated with LBA production rates =		130.1	3.0	126.6	5.9	190.9	4.4	24.8	178.5	8.4	32.3	186.3	19.7	186.3	20.0
LBA-01-66§§					Calculated with LBA production rates =		103.5	2.4	90.6	4.6	136.8	3.1	16.0	112.9	5.7	18.4	126.5	12.1	126.4	12.2
Telken V moraine																				
LBA-01-48	631	30-35	46° 50′ 14.7″	70° 43′ 36.2″	22.69 ± 0.528	89.180 ± 26.993	220.6	5.1	144.9	44.2	Erosion rate = 2.3 ± 0.1 mm/kyr##									

Notes: All samples corrected for thickness of 1.5 cm (scaling = 0.9866), except LBA-98-135 (2 cm), and no shielding correction required. Effective geomagnetic latitude used: 46.77°S for 19–15 ka, 47.47°S for 25–20 ka, and 46.5°S for Moreno/Telken samples (see text). Attenuation length (Brown et al., 1992): 145 ± 7 g cm^{-2} (^{10}Be) and 156 ± 12 g cm^{-2} (^{26}Al). Procedural blanks: ^{10}Be = 1.45 and 2.18 × 10^{-14}; and ^{26}Al = 2.38 and 3.80 × 10^{-15}.

†Age 1 calculated with zero erosion rate.

‡Age 2 calculated with erosion rate 2.3 ± 0.1 mm/k.y. (see text). All ages calculated with ''global'' rates 5.1 and 31.1 atoms/gm/yr (Stone, 2000). In addition, for two Moreno samples, Age 2 calculated with LBA long-term rates 5.9 and 35.8 atoms/gm/yr, respectively (see text; Ackert et al., 2003).

§Individual boulder ages based on Age 2, with ^{10}Be and ^{26}Al measurements weighted inversely by their own variances (excluding Al age for LBA-98-98).

#Error includes propagation of analytical uncertainties (AMS and ICP-AES; latter only for Al).

††Error includes propagation of analytical uncertainties, uncertainties for erosion rate (2.3 ± 0.1 mm/kyr), rock density (±0.1 g cm^{-3}), and attenuation length (see above notes). Errors propagated step-by-step while solving age equation (see text).

‡‡Calculated same as error to left, except also includes propagation of production rate uncertainty; ±6% for Fenix V–IV (see text), ~3% for Fenix II–I (Stone, 2000); and ~1.5% for Moreno samples (see text). Mean boulder ages slightly different than those to left because sample ages are weighted inversely by different variances.

§§Ages and errors based on local LBA long-term production rate (see text; Ackert et al., 2003).

##Erosion rate based on ^{40}Ar/^{39}Ar ages of Telken and Arroyo Page lavas (Singer et al., 2004), ^{10}Be nuclide concentration, and LBA long-term production rate.

TABLE 3. CHEMICAL COMPOSITION OF BASALTIC BOULDERS ON FENIX AND MORENO MORAINES

Sample	Basalt lithology†	SiO_2 (%)	Al_2O_3 (%)	CaO (%)	MgO (%)	Na_2O (%)	K_2O (%)	Fe_2O_3 (%)	MnO (%)	TiO_2 (%)	P_2O_5 (%)	Cr_2O_3 (%)
LBA-98-068A	2	48.22	14.26	6.2	5.68	4.18	1.99	12.11	0.14	1.83	0.8	0.04
LBA-98-074	1	48.49	14.77	7.46	7.66	3.31	1.3	12.79	0.16	1.98	0.49	0.04
LBA-98-075	1	48.44	14.54	7.06	7.44	3.48	1.17	12.47	0.16	1.99	0.52	0.04
LBA-98-085, 087	1	47.72	14.25	7.06	7.29	3.41	1.42	12.45	0.15	1.96	0.75	0.04
LBA-98-090	1	48.34	14.77	7.72	7.79	2.87	1.29	12.78	0.17	2.09	0.46	0.04
LBA-98-099	1	47.57	14.21	7.27	7.43	3.49	1.3	12.62	0.16	1.98	0.52	0.04
LBA-98-116	2	48.34	14.91	6.42	5.94	4.17	1.68	12.42	0.14	1.88	0.84	0.03
LBA-98-134A, B	3	48.33	15.69	10.09	8.85	2.7	0.41	12.44	0.19	1.17	0.11	0.06
LBA-98-136	1	48.49	14.74	7.46	7.52	3.48	1.18	12.63	0.16	1.98	0.48	0.04

†Lithology 1 is 16.8 Ma basalt, lithology 2 is undated, and lithology 3 is 117.5 Ma lithology. See text.

grains are clear to light yellow with no visible inclusions. The boulders exhibit well-developed columnar jointing with individual columns 10–15 cm wide. The second lithology appears similar to the first in hand specimens but has distinctly higher Na and K and lower Ca and Mg concentrations (Table 3). The third lithology is coarse-grained basalt with up to 4% olivine phenocryrsts containing abundant inclusions. Boulders composed of this lithology also have columnar joints, but the columns are larger, typically 20–30 cm wide. Previous $^{40}Ar/^{39}Ar$ dating has shown that the first and last lithologies have ages of 16.8 Ma and 117.5 Ma, respectively (Ton-That et al., 1999).

Samples shielded from cosmic ray bombardment by >2 m of rock were obtained from the underside of the largest boulders of two lithologies to correct for inherited ^3He concentrations (see below). Sample LBA-98–087 was obtained from beneath a block of the 16.8 Ma lithology, which split off of the side of the parent boulder (Sample LBA-98–085) (Fig. 3C). Extremely well preserved glacial polish and striations on the underside of the block indicate that calving occurred soon after deposition of the parent block, but the measured ^3He must include a small cosmogenic component. Sample LBA-98–134B is from under a large (<5 m) block of the 117 Ma lithology (Sample LBA-98–134A) that has split into two (Fig. 3F). Although this sample is partially shielded by the companion block and >1 m in from the bottom edge, it also must contain a small cosmogenic ^3He component.

Olivine phenocrysts for ^3He measurements were separated from the groundmass by crushing, sieving, magnetic separation, and handpicking. Helium isotopes released by melting ~60 mg of olivine were measured on the helium mass spectrometer at the Woods Hole Oceanographic Institution (MS 2) using previously described techniques (Kurz, 1986; Kurz et al., 1996). Sample size (^4He concentration) and $^3He/^4He$ are measured relative to an air standard with reproducibility of less than 0.5% and 1.5%, respectively. System blanks were less than 1.5×10^{-10} ^4He ccSTP. Furnace blanks were measured for each furnace load and varied from 1×10^{-10} to 2×10^{-10} ^4He ccSTP.

To calculate ^3He exposure ages, the ^3He concentrations specifically due to cosmogenic production must be determined. Typically, olivine separates are crushed under vacuum to selectively release magmatic helium trapped in fluid inclusions. The crushed powders are then melted under vacuum to release the remaining helium (Kurz, 1986; Kurz et al., 1996). The cosmogenic ^3He concentration is determined by subtracting the magmatic component from the total ^3He.

$$^3He_c = {}^3He_t - {}^3He_{i,} \quad (1)$$

where ^3He_c is cosmogenic, ^3He_t is total released on melting, and ^3He_i is inherited (magmatic) ^3He. ^3He_i and ^3He_t are determined as follows:

$$^3He_i = {}^3He/{}^4He_{cr} \times {}^4He_m \quad (2)$$

$$^3He_t = {}^3He/{}^4He_m \times {}^4He_m, \quad (3)$$

where *cr* denotes values obtained by crushing and m denotes values obtained by melting residual powders. Equation 2 assumes that all ^4He is magmatic, specifically $^4He_i >> {}^4He_c$, and that there are no other ^4He components. However, this assumption is only valid for young basalts. In older basalts, such as those analyzed here, inherited ^4He produced radiogenically during decay of U and Th and ^3He generated by the thermal neutron capture reaction $^6Li(n, \alpha)T \rightarrow {}^3He$ (Kurz, 1986; Cerling and Craig, 1994) potentially become significant. For some Lago Buenos Aires samples, cosmogenic ^3He concentrations calculated as above yield negative ages, clearly indicating that the assumption of only magmatic ^4He is invalid.

An additional complication is that radiogenic ^4He distributions are not homogenous. U and Th primarily reside in the groundmass of basalt. Because the stopping distance of an alpha particle is ~20 μm, radiogenic ^4He is concentrated near the surface of olivine grains (Farley et al., 1996). Total ^4He concentrations in olivine depend on grain size, the distribution of U and Th, and the amount of original surface retained in the measured grains.

Olivine phenocrysts 500–1000 μm in diameter were abraded in N_2 (Krogh, 1982) to remove rims containing elevated radiogenic and nucleogenic He components and obtain cores with presumably consistent, homogenous He concentrations and isotope ratios. In an experiment in which the olivine was subject to increasing degrees of abrasion, both ^3He and ^4He concentrations decrease with increasing abrasion, consistent with removal of a He-enriched rim of the olivine grains (see samples LBA-98–090a–d, Table 4). Although it is not clear that only core material free of implanted radiogenic ^4He and nucleogenic ^3He remained at the end of the abrasion process (concentrations did not level off), the experiment suggests that this is a valid approach. Typically, this abrasion process removed half of the starting sample mass; however, this does not mean that half of each grain was removed. Initially, the abraded samples were both crushed and melted. Later on, samples were melted without crushing.

From the shielded samples, inherited ^3He and ^4He concentrations were determined in abraded samples from the 16.8 and 117.5 Ma basalt lithologies. Cosmogenic ^3He concentrations were obtained by two methods: (1) Subtracting the total ^3He concentration obtained from abraded, shielded samples from the total ^3He measured in the exposed samples; (2) Substituting the $^3He/^4He$ of the shielded sample for $^3He/^4He_{cr}$ in Equation 2. Similar ages obtained using both methods would indicate that the assumptions concerning the helium distributions in the minerals are correct. This is the case for the boulders from which shielded samples were obtained; these ages are also

TABLE 4. HE DATA FROM MORAINE BOULDERS IN LAGO BUENOS AIRES, 46.5°S

Sample	Basalt lithology	Elevation (m)	Height (cm)	Latitude (°S)	Longitude (°W)	Crush		Melt		Age 1 ± 1σ (ka)	Age 2 (ka)	Age 3 (ka)
						$^3He/^4He \pm 1\sigma$ (R/R_a)	$^4He \pm 1\sigma$ (atom/g × 10^{10})	$^3He/^4He \pm 1\sigma$ (R/R_a)	$^4He \pm 1\sigma$ (atom/g × 10^{10})			
Menucos												
LBA-98-116	3	390	350	46°36.046′	71°04.019′	2.59 ± 1.74	1.84 ± 0.04	4.25 ± 0.11	55 ± 0.1	19.5 ± 0.6		
Fenix I												
LBA-98-068A	3	440	300	46°35.904′	71°02.127′	Not crushed		3.22 ± 0.06	119 ± 0.2	29.9 ± 0.6		
LBA-98-074	1	440	450	46°35.502′	71°02.209′	2.25 ± 0.10	11.3 ± 0.0	0.33 ± 0.01	827 ± 1.5	23.2 ± 0.1	10.5	−83.3
LBA-98-075	1	440	450	46°35.181′	71°02.299′	3.04 ± 0.15	24.4 ± 0.1					
						1.67 ± 0.44	3.33 ± 0.02	7.2 ± 0.13	44.3 ± 0.1	31.1 ± 0.5	18.4	21.9
Fenix II												
LBA-98-085	1	438	1400	46°35.871′	71°01.542′	Not crushed		5.3 ± 0.06	80.5 ± 0.1	33.3 ± 0.4	20.6	23.1
LBA-98-087 (shielded)	1	435	60	46°35.871′	71°01.542′	Not crushed		1.63 ± 0.05	100 ± 0.2	12.8 ± 0.4		
LBA-98-090-a	1	426	350	46°37.243′	71°01.606′	2.84 ± 0.19	99.0 ± 0.3	1.56 ± 0.04	213 ± 0.4	48.4 ± 1.6	35.6	8.3
LBA-98-090-b	1	426	″	″	″	2.41 ± 0.05	90.1 ± 0.2	1.92 ± 0.02	175 ± 0.4	43.7 ± 0.5	30.8	9.6
LBA-98-090-c	1	426	″	″	″	3.37 ± 0.06	36.1 ± 0.1	3.13 ± 0.06	124 ± 0.2	40.2 ± 0.6	27.4	19.7
LBA-98-090-d	1	426	″	″	″	1.81 ± 0.09	33.1 ± 0.1	3.20 ± 0.05	101 ± 0.2	30.3 ± 0.5	17.5	13.0
LBA-98-099	1	431	200	46°33.337′	71°01.614′	4.10 ± 0.78	1.84 ± 0.03					
						3.48 ± 0.37	5.42 ± 0.02	7.75 ± 0.10	40.9 ± 0.1	27.0 ± 0.4	14.1	21.0
Fenix V												
LBA-98-136	1	440	500	46°37.377′	70°57.450′	3.16 ± 0.26	13.8 ± 0.05	11.9 ± 0.2	35.2 ± 0.1	36.0 ± 0.5	23.3	29.8
Moreno I												
LBA-98-134A	2	440	750	46°37.390′	70°55.510′	7.53 ± 0.74	4.78 ± 0.04	23.0 ± 0.1	96 ± 0.3	153 ± 1	131	136
								Erosion rate = 2.3 mm/k.y.		238 ± 2	187	197
								With global production rate		297 ± 3		
LBA-98-134B (shielded)	2	437	50	46°37.390′	70°55.510′	7.07 ± 0.29	11.5 ± 0.1	2.37 ± 0.04	100 ± 0.2	21.9 ± 0.4		
								2.61 ± 0.06	120 ± 0.2	21.5 ± 0.5		

Notes: Lithology 1 is 16.8 Ma basalt; lithology 2 is 117.5 Ma lithology; and lithology 3 is undated. See Table 3. R/Ra is $^3He/^4He$ of air = 1.384 × 10^{-6}. Errors are propagated analytical uncertainties only. Age 1 is maximum age, assumes all ^3He is cosmogenic. Age 2 corrects for inherited ^3He using total ^3He of shielded samples. Age 3 corrects for inherited ^3He using $^3He/^4He$ of shielded samples. LBA-98-087 and LBA-98-134B are shielded samples. LBA-98-075 and LBA-98-099 were crushed twice.

in reasonable agreement with the ^{10}Be-^{26}Al boulder ages from the same moraine. Less consistent results were obtained for most of the other boulders, implying the helium distribution is other than assumed. Possibilities include partial retention of grain rims after abrasion or heterogeneous distribution of U- or Th-bearing inclusions. Given the large uncertainties in applying the corrections from the shielded samples, maximum exposure ages that assume all ^3He is cosmogenic are also presented; these ages are robust and support the conclusions based on the other cosmogenic nuclides.

Production Rates

Although analytical uncertainties in measuring cosmogenic nuclides are commonly less than 4% (Tables 2 and 4; all errors hereafter are 1σ unless otherwise stated), geologic uncertainties, including boulder movement, erosion, and snow cover associated with surface exposure dating may be much higher and are reflected in the scatter of determined ages (Gosse and Phillips, 2001). In addition, systematic uncertainties associated with calibration of production rates of cosmogenic nuclides, combined with scaling these rates to sea level and high latitude (SLHL), are estimated to be as high as 10–20% (see Gosse and Phillips, 2001). It should be emphasized that even a systematic uncertainty of 10–20% would not change the major conclusions presented in this paper.

We adopt the ''global'' production rates of 5.1 ± 0.3 atoms/gm/yr for ^{10}Be and 31.1 ± 1.9 atoms/gm/yr for ^{26}Al (both rates ± 2σ; SLHL and standard atmosphere) and assume a muogenic component of production of 0.026% and 0.022% at sea level for each nuclide, respectively (Stone, 2000; Gosse and Stone, 2001). Similarly, a global rate of 120.6 ± 4.8 atoms/gm/yr (SLHL and standard atmosphere) for ^3He was adopted based on the weighted mean of concentrations in Bonneville flood deposits and Tabernacle Hill lava flows corrected for local pressure (Cerling, 1990; Licciardi et al., 1999; Stone, 2000). Scaling with altitude follows equation 1 and Table 1 in Stone (2000), accounting for a present mean annual sea level pressure of 1009.32 hPa and an annual temperature of 8 °C (Taljaard et al., 1969). This pressure and temperature cause a ~3.6% increase in global production rates at sea level at 46.5 °S (cf., Fig. 1 *in* Stone [2000]). These are the same production rates that gave concordant ^{10}Be and ^3He ages for granite and basalt boulders on the Eight Mile moraine at Yellowstone (Licciardi et al., 2001). Moreover, the use of global production rates (i.e., Stone, 2000) yields exposure ages for the youngest Fenix moraine (see below) that are consistent with the ^{14}C ages obtained from the overlying varved sediment (Tables 1 and 2; Fig. 4). In addition, it must be kept in mind that the carbonate-cemented concretion ^{14}C data have not been corrected for possible reservoir effects (e.g., due to ''old'' C in groundwater); presently, the magnitude of a potential effect is unknown.

Scaling factor and production rate uncertainties are minimized for Fenix moraine samples for the following reasons. First, the Lago Buenos Aires sampling sites lie close in latitude to most published calibration sites (e.g., Nishiizumi et al., 1989; Gosse and Stone, 2001). Thus, scaling of the production rates at the calibration sites to SLHL, to estimate ''global'' production rates, involves a similar standardization as scaling from SLHL to Lago Buenos Aires sites. Second, in other studies, the Lal (1991)-based scaling used here captures the altitude dependence of the production rate within the analytical uncertainties (Zreda, 1994; Ackert et al., 2003). Third, most exposure ages presented for the Fenix moraines are similar to calibration site ages, <17 ka, thus, uncertainties introduced by time-dependent variations in production rates are small.

For Moreno moraine samples, we use a locally derived long-term production rate, which limits scaling and production rate uncertainties to as low as ~5% because the local calibration sites are from lava flow surfaces similar in age (68 ka and 109 ka) and elevation

(900 m and 500 m) to the moraine boulders (Ackert et al., 2003). This local ^{3}He production rate (136.7 ± 3.5, 2σ) is ~11% higher than published calibrations and is attributed to lower atmospheric pressure at Lago Buenos Aires during glacial climates (Ackert et al., 2003). Because ^{10}Be and ^{26}Al are also produced dominantly by spallation, we scale the ^{10}Be and ^{26}Al production rates accordingly. For comparison, the Moreno ages are also derived and shown in Table 2 and Figure 4 with global production rates (Gosse and Stone, 2001; Licciardi et al., 1999).

It is important to scale global production rates (e.g., Stone, 2000) to an effective geomagnetic latitude (Nishiizumi et al., 1989; Lal, 1991) to account for changes in the magnetic field over the exposure history of the sample. Although fluctuations in the intensity and inclination of the geomagnetic field over the past ~100 k.y. are assumed to have had a small impact on production rates—and hence uncertainty—in cosmogenic dating at Lago Buenos Aires, it is worthwhile to outline the scaling done here. Proxy records of paleointensity include Guyodo and Valet (1999), Ohno and Hamano (1993), and McElhinny and Senanayake (1982). The SINT800 paleointensity record of Guyodo and Valet (1999) was used, except for the last 11 k.y. For the period between 11 and 10 ka, McElhinny and Senanayake's (1982) intensity values were used, whereas for the last 10 k.y. estimates from Ohno and Hamano (1993) are preferred, in part because they include data from Argentina. Over the last 25 k.y. (i.e., Fenix time), the integrated effect of magnetic field changes on exposure ages is small, and the estimated geomagnetic latitude varied from ~47.5 to 46.8°S between 25 and 15 ka.

In general, non-dipole effects at 46°S latitude and 400–500 masl may change production rates by <2%, and furthermore, they are insignificant for moraines greater than 20 ka (Gosse and Phillips, 2001; Dunai, 2001). However, there is presently a strong inclination anomaly over the South Atlantic–South American region, such that data from Ohno and Hamano (1993) may not fully compensate for this effect at Lago Buenos Aires over the last 20 k.y. (Dunai, 2001). Dunai (2000) proposed an alternative scaling scheme that includes time-dependent non-dipole components of the magnetic field and uses atmospheric attenuation lengths different than those of Lal (1991). We chose the Stone (2000) scaling scheme for Fenix samples because it relies on the relations of Lal (1991), which better capture the altitude dependence of production rates in this area (Ackert et al., 2003).

For Moreno "time" (>109 ka), directional effects are small or insignificant (Gosse and Phillips, 2001). A theoretical estimate of the total integrated effect of changes in magnetic inclination and intensity at 46.5°S on production rates is <0.5% for any period prior to 25 ka (Masarik et al., 2001). Alternatively, using an empirical correction (cf., Nishiizumi et al., 1989), as was done above for Fenix samples, may increase Moreno ages by as much as 3% (Table 2). We emphasize that correction of the local Lago Buenos Aires long-term production rate of Ackert et al. (2003) for magnetic field variation is not required for Moreno samples because the sites are from a similar altitude and within 10 km of the Cerro Volcán calibration area.

TABLE 5. WEIGHTED MEAN ^{10}Be-^{26}Al AGES

Moraine	Age (ka)†		Age (ka)‡	
	Mean	±1σ	Mean	±1σ
Fenix I	15.6	1.1	15.6	1.1
Fenix II	18.7	1.0	18.7	1.0
Fenix III	20.7	1.3	20.6	1.4
Fenix V	23.0	1.2	22.9	1.3

†Means based on boulder ^{10}Be-^{26}Al ages that include propagation of all uncertainties except for production rate (Table 2). These values are used in Figure 4.

‡Means based on boulder ^{10}Be-^{26}Al ages that include propagation of all uncertainties including production rate (Table 2). These values are used in Figure 5. Mean ages are slightly different than those to left because different errors are weighted. ^{26}Al ages have larger error bars and are often younger than ^{10}Be ages, and thus they have greater influence on weighted mean calculation when production rate errors are included in propagation of errors.

Erosion Rate

Quantifying boulder erosion rate is essential to correct for the removal of some cosmogenically produced atoms and is an ongoing objective at Lago Buenos Aires. Erosion rates are expected to vary nonuniformly both temporally and spatially. A provisional estimate of boulder erosion rate (2.3 ± 0.1 mm/k.y.) is based on the ^{10}Be concentration in a granite boulder on the Telken V moraine (LBA-01–48; Fig. 2, Table 2). Given the large uncertainty of the ^{26}Al concentration (Table 2), this exercise was done only with the ^{10}Be concentration. The two "unknowns" that determine cosmogenic nuclide concentrations are time and erosion rate (Lal, 1991). Because the age of the Telken V moraine is stratigraphically bracketed between the ^{40}Ar/^{39}Ar-dated Arroyo Page (760 ka) and Telken (1016 ka) flows (Singer et al., 2004), "time" is known and the age equation can be solved for erosion rate. The ^{10}Be concentration is apparently close to steady state, where nuclide accumulation is equal to loss by radioactive decay and erosion (Lal, 1991), such that the calculated erosion rate is insensitive to whether the Arroyo Page or Telken flow ages are used. For comparison, assuming steady state (Lal, 1991), the erosion rate derived is 2.4 mm/k.y.

As the rate of 2.3 mm/k.y. strictly applies only to boulder LBA-01–48, caution must be used when extrapolating throughout the Lago Buenos Aires area; thus, ages from Moreno moraine boulders remain tentative. In fact, uncertainty in the rate of erosion is presently the factor that most limits the accuracy of surface exposure ages for the Moreno moraine. An erosion rate of ~2.3 mm/k.y. is consistent with erosion rates found in other semi-arid regions (0.5–12 mm/k.y.; see compilation by Small et al., 1997). Applying an erosion rate of 2.3 mm/k.y. increases ages by ~2.2% and ~3.6% for Fenix I and V samples, respectively, but increases ages of the Moreno samples by more than 25%.

The erosion rate determined from the LBA-01–48 boulder on the Telken V moraine is influenced by the production rate used. Given its antiquity, we use the newly derived long-term Lago Buenos Aires production rate. However, if the production rates of Stone (2000) were applied to the LBA-01–48 ^{10}Be concentration (and accounting for present atmospheric pressure), then the erosion rate would be ~2.0 mm/k.y. An erosion rate of 2.0 rather than 2.3 mm/k.y. would decrease the ^{10}Be ages of LBA-01–62 and LBA-01–66 by ~8.5% and 5.6%, respectively.

Final Age Calculation and Uncertainties

Following the systematic adjustments outlined above, the age of each boulder was calculated (Table 2) by weighting both the ^{10}Be and ^{26}Al ages by the inverse variance (Taylor, 1982). The ^{26}Al age of sample LBA-98–98 is the only measurement not included in a boulder age calculation because it is distinctly younger than the respective ^{10}Be age and those of all other boulders on Fenix II. The mean age of each Fenix moraine was then calculated (Table 5) by weighting all of the individual boulder ages (i.e., ^{10}Be-^{26}Al) by the inverse variance. The maximum ^{3}He ages are all older than the ^{10}Be and ^{26}Al ages. Although the ^{3}He ages based on the shielded samples are commonly consistent with the ^{10}Be-^{26}Al ages, these are not plotted on the figures of Fenix moraine ages, nor are they included in the weighted mean moraine ages (Table 5), because of the poorly constrained uncertainties associated with the correction for inherited ^{3}He.

Unless otherwise mentioned, all total cos-

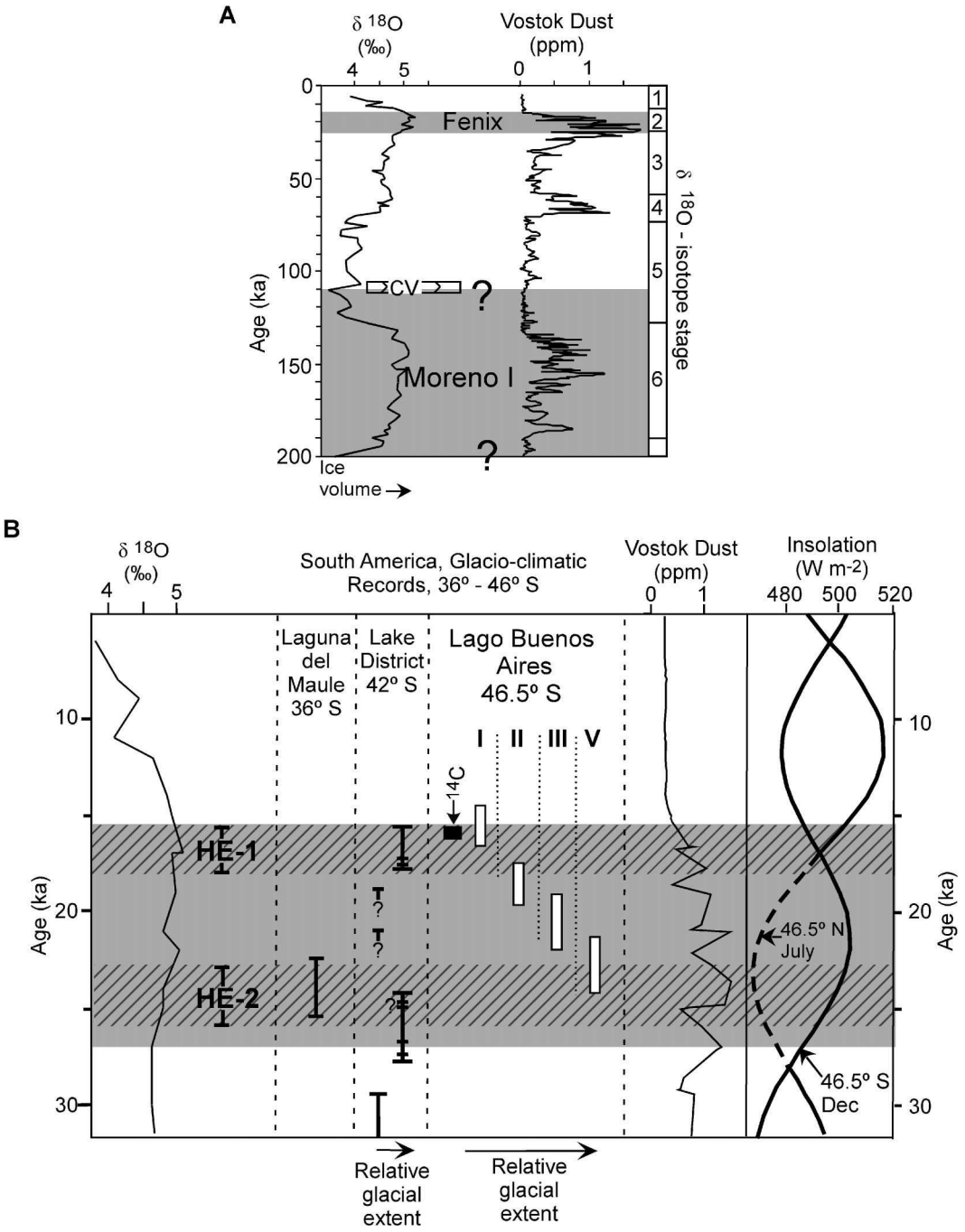

Figure 5. Lago Buenos Aires record compared with changes in Northern Hemisphere ice sheets (i.e., $\delta^{18}O$), Vostok dust concentration, other mid-latitude South American glacial geologic records, and insolation. (A) For comparison, over last 200 k.y., $\delta^{18}O$ (Shackleton et al., 1990) Vostok dust concentration (Petit et al., 1999) and timing of major glacial periods recorded at Lago Buenos Aires are shown. Range of cosmogenic nuclide ages for Fenix and Moreno moraine systems represented by gray bands. The 109 ka age of Cerro Volcán (CV) is also shown for comparison. Note major hiatus between formation of Fenix and Moreno systems. Question marks reflect age uncertainty of Moreno I. (B) For comparison, over last ~30 k.y., $\delta^{18}O$, timing of two coldest periods in North Atlantic region partly represented by Heinrich events (HE) 2 and 1 (Elliot et al., 1998; calendar ages based on Stuiver et al. [1998] and Beck et al. [2001]), glacial advance at Laguna del Maule (Singer et al., 2000), glacial advances/cool periods in Lake District (Heusser et al., 1999; Denton, 1999), glacial record at Lago Buenos Aires, Vostok dust concentration (Petit et al., 1999), and insolation in both hemispheres (Berger and Loutre, 1991). Gray band reflects period of major glacial expansion in both hemispheres and hashed lines show timing of Heinrich events in North Atlantic region. Relative glacial extent is shown from Andean divide. For Lago Buenos Aires, white vertical bars indicate weighted mean moraine ages that include boulder ages with propagation of production rate uncertainties (Table 5). For Lake District, wider outer error bars bracket cool periods (Heusser et al., 1999) and narrower inner error bars bracket glacial advance maxima (Denton et al., 1999); some glacioclimatic events are shown, schematically, as being about same extent relative to Andean divide. Note that for all three South American sites, maximum glacial extent is observed prior to ca. 22 ka and likely between 27 and 22 ka, and in some areas at ca. 18–17 ka (Denton et al., 1999).

mogenic age uncertainties (± 1σ) discussed include propagation of uncertainties associated with the Accelerator Mass Spectrometry ($^{10}Be/^{9}Be$, $^{26}Al/^{27}Al$), Rare Gas Mass Spectrometry (^{3}He), ICP-AES analyses of Al concentration, erosion rate (±0.1 mm/k.y.), rock density (± 0.1 g/cm^3), and attenuation length (Table 2). For correlation to records outside of Lago Buenos Aires (i.e., for Fig. 5), production rate uncertainties (±1.5–6%; see Table 2) are also propagated to reflect uncertainties in published rates (e.g., Gosse and Stone, 2001) and data in Ackert et al. (2003), which indicate that changes in air pressure may have reduced the production rate slightly from Fenix V to Fenix I time. Errors were propagated, conservatively, step-by-step using sum in quadrature and power rules in Taylor (1982;

equations 3.18 and 3.26) as we solved the respective age equations. If instead the general rule for error propagation was used and total uncertainty calculated in one step (Taylor, 1982), errors would decrease on average by ~30–40% for Fenix samples and 80% for Moreno samples.

RESULTS

Moreno Moraine Complex

The limited number of samples, low boulder height of the samples, and provisional erosion rate lead us to suggest only a ''best estimate'' age range between ca. 200 and 120 ka for deposition of the Moreno I moraine. Using the local long-term production rate, two small samples from the Moreno complex provide ^{10}Be-^{26}Al ages of 129 and 101 ka (erosion rate = 0 mm/k.y.) or 186 and 127 ka (2.3 mm/k.y.), clearly distinguishing a temporal gap between deposition of the Moreno and Fenix moraines (Table 2; Figs. 4 and 5). Moreover, the ^{10}Be-^{26}Al ages of boulder LBA-01–66 are consistent with its stratigraphic relationship to the overlying 109 ± 3 ka (2σ) Cerro Volcán flow, provided an erosion rate of between 1.0 and 2.3 mm/k.y. is assumed.

Assuming no erosion, the ^{3}He exposure age of Moreno basalt sample LBA-98–134A was determined to be between 153 and 131 ka, depending on assumptions about inherited ^{3}He (Table 4). Because the correction for inheritance is relatively small (14%), the LBA-98–134A ^{3}He data are shown in Figure 4. Applying an erosion rate of 2.3 mm/k.y., the LBA-98–134A age, corrected for shielding, is 197–187 ka. The latter ^{3}He age is indistinguishable from the ^{10}Be-^{26}Al age of boulder LBA-01–62 (Fig. 4) but older than boulder LBA-01–66 (for erosion rates between 0 and 2.3 mm/k.y.). Thus, it may be that LBA-01–62 and LBA-01–134A, which are relatively tall boulders, give older ages owing to reduced burial compared to LBA-01–66, which is only 5 cm tall. Further analyses under way will address these issues for the Moreno moraines.

Fenix Moraine Complex

The new AMS age of the concretion of 12,880 ± 160 ^{14}C yr B.P. (± 1σ) is consistent with the two ^{14}C ages previously obtained by Sylwan (1989). The three ^{14}C ages on lacustrine varves at Lago Buenos Aires (Table 1) range from 14.1 to 12.9 ^{14}C yr B.P., corresponding to ~16.9–15.5 ka (all ^{14}C ages hereafter are calendar years ± 1σ [Stuiver et al., 1998]). Taken at face value, the ^{14}C data provide a minimum age for the underlying Fenix I moraine and a maximum age for the overlying Menucos moraine (Fig. 4). Although these ^{14}C ages may be maxima for the carbonate concretions, as they are not corrected for reservoir effects, when calibrated, they are consistent with the cosmogenic ages presented below for Fenix I.

Individual ^{10}Be-^{26}Al boulder ages for the Fenix moraines range from 23.6 to 12.5 ka (erosion rate = 0 mm/k.y.) or 23.9 to 12.8 ka (erosion rate = 2.3 mm/k.y.). The ^{10}Be ages are more precise than the respective ^{26}Al ages on the same boulders and strongly influence the weighted mean boulder ages, especially if erosion and production rate errors are not propagated (Table 2). On a given Fenix moraine, all ^{10}Be-^{26}Al boulder ages overlap within the 1σ propagated uncertainties. The age coherence for samples from different locations along each moraine crest and the excellent conformity with the relative age sequence (Fig. 4) indicate that inheritance from exposure prior to deposition on the landscape, or burial, do not appear to be a major problem at Lago Buenos Aires.

The total ^{3}He surface exposure ages (Table 4) provide maximum age estimates that range from 36.0 to 19.5 ka, which mirror the increase of ^{10}Be-^{26}Al boulder ages from Fenix I to V. In general, the inheritance-corrected ^{3}He ages (Age 2 and Age 3, Table 4) fall within a few thousand years of the ^{10}Be-^{26}Al ages but are typically older. It is evident that the corrections required for inherited ^{3}He are considerable, ~40% for the fine-grained basalt, and vary with lithology (Tables 3 and 4). The scatter is attributed to insufficient abrasion of sample olivine populations and retention of varying amounts of the helium-enriched rims of the grains. Therefore, the ^{3}He ages are not included in the mean moraine age calculations (Table 5). The results indicate that determining young exposure ages on old basalts using ^{3}He can be difficult. However, the technique can reveal important chronologic information, especially if quartz-rich samples are lacking. The likelihood of more precise results would be greater given larger and more abundant olivine phenocrysts than were available in these boulders.

DISCUSSION

Recent Glacial History of Mid-latitude Andes, ~36–46°S

The new cosmogenic nuclide data refine the broad age constraints for seven of the youngest moraines based on ^{40}Ar/^{39}Ar ages and stratigraphic relationships (Ton-That et al., 1999; Singer et al., 2004). In addition, the coherency between ^{14}C, ^{10}Be, ^{26}Al, ^{3}He, and ^{40}Ar/^{39}Ar data suggests that geologic uncertainties described above are minimized to the point that cosmogenic dating has exceptional potential for reconstructing the Lago Buenos Aires glacial history.

Individual Lago Buenos Aires moraine ages and precise one-to-one correlations with paleoclimatic events in other southern South America records must be considered tentative and require testing with further reduction of systematic and geologic uncertainties. As the sources of error are diminished in the future, cosmogenic ages calculated on the basis of our present understanding will need to be further revised. We do not anticipate that the magnitude of potential age corrections will exceed ~11% (e.g., Ackert et al., 2003). Furthermore, we reiterate that despite present uncertainties, our fundamental conclusions will not change in the future if the chronology is refined.

Prior to 25 ka

As previously mentioned, our age assignments prior to ca. 25 ka are tentative. Based on the overlying Cerro Volcán lava flow and three cosmogenic ages, we can confidently assign a limiting minimum age of Moreno I greater than 109 ka, although we estimate that deposition occurred between ca. 200 and 120 ka. The most reasonable interpretation of the cosmogenic data is that at least part of the Moreno moraine complex was deposited during marine δ^{18}O isotope stage 6 (190–130 ka). Until now, direct evidence of a major glaciation during stage 6 in the Andes has been difficult to verify (Clapperton, 1993). A stage 6 glaciation at Lago Buenos Aires is consistent with the volcanic geology at 36°S, where the Tatara-San Pedro complex (Fig. 1) exhibits a prominent gap in the lava record at this time that is thought to reflect a major episode of glacial erosion (Singer et al., 1997).

We consider it unlikely that the youngest part of the Moreno moraine was deposited during stage 5d (ca. 115 ka), which could be inferred based on the youngest exposure age, LBA-01–66 (Fig. 4). As discussed above, assuming an ideal exposure history for this low boulder (Table 2) is questionable. In addition, glacial-age dust in the Vostok ice core, which has a distinct Patagonian Sr, Nd, and Pb isotope signature (Basile et al., 1997; Petit et al., 1999), does not support a 5d glacial event. While dust concentration does not show an appreciable increase during stage 5d (or anywhere between ca. 130 and 100 ka), maxima

do occur during stages 6, 4, and 2, (Fig. 5A). We suggest that an elevated Vostok dust concentration should be observed if part of Moreno I was deposited ca. 115 ka, in light of the similar Andean glacial extent required to form Moreno I and the stage 2 Fenix moraines (Figs. 2, 3F, and 5A).

There are no sites in southern South America where it can be demonstrated conclusively that glaciogenic deposits formed during stage 4, ca. 75 ka (Clapperton, 1993). The available data (Figs. 2 and 4) suggest that stage 4 moraines are not preserved at Lago Buenos Aires. However, glacial-age dust in the Vostok ice core (Fig. 5A) provides strong evidence that during stage 4, Patagonian glaciers did advance (Basile et al., 1997; Petit et al., 1999). Apparently, Fenix ice advances during stage 2 obliterated any previous stage 4 deposits (Figs. 2 and 4). For comparison, in the southern Andes at 36°S, the K-Ar- and $^{40}Ar/^{39}Ar$-dated record of volcanism at the 3600-m-high Tatara–San Pedro complex (Fig. 1) implies that glaciation during stage 4 was less intense than that during stages 6 and 2 (Singer et al., 1997).

After 25 ka

The new chronological data (Fig. 4) indicate that the five Fenix ice advances occurred between ~23 and 16 ka and imply that the Patagonian ice cap was responding to millennial-scale climate forcing during stage 2, a period of high summer insolation (Fig. 5B). In fact, there is consistent evidence of major ice expansion between ca. 27 and 15 ka throughout the southern Andean Cordillera (Fig. 5B; Denton, 1999; Clapperton and Seltzer, 2001). Furthermore, records from mid-latitude South America (Fig. 5B) indicate that Andean outlet glaciers reached their maximum extent in most areas between ca. 27 and 22 ka (Fig. 5B), with exceptions peaking at ca. 18–17 ka (Denton et al., 1999). Although we hesitate to assign precise absolute ages to individual Lago Buenos Aires moraines, the temporal pattern is consistent with the cool periods/glacioclimatic maxima in the Lake District (Fig 5B).

A similar finding occurs at Laguna del Maule (Fig. 1), 1000 km north of Lago Buenos Aires, where $^{40}Ar/^{39}Ar$ dating of glaciated and unglaciated lava flows demonstrates that the last major ice advance took place between 25.6 ± 1.2 ka and 23.3 ± 0.6 ka (Singer et al., 2000). Evidence for a subsequent readvance is absent at this latitude. We infer that after ca. 23 ka, Laguna del Maule—at 36°S and at ~2150 m asl—must have been below the ''glacial-age'' snow line for this area based on estimates that place it between ~2500 and 3000 m (Broecker and Denton, 1989). Singer et al. (2000) concluded that the lack of glacial advances after ca. 23 ka possibly reflects the start of southerly migration of the Westerlies toward their present interglacial position (Fig. 1).

Deglaciation from the Fenix I moraine occurred after ca. 16 ka. The Lago Buenos Aires glacier then had retreated such that an ice-dammed proglacial lake was impounded behind the Fenix I moraine and, subsequently, a readvance took place, depositing the Menucos moraine (Singer et al., 2004). Presently, we have no direct age constraints for the Menucos moraine other than a single ^{3}He exposure of < 19 ka. Southwest of the study area, Mercer (1976) obtained a ^{14}C age of 11.2 ± 0.2 ^{14}C yr (13.2 ka), which provides a minimum age for the opening of the Rio Baker outlet to the Pacific Ocean and ice recession from the Lago Buenos Aires basin and, thus, formation of the Menucos moraine. In any case, deglaciation in the Lago Buenos Aires basin occurred sometime after or ca. 16 ka, lagging the local insolation maximum by at least 5 ky (Fig 5B). The timing of the last Lago Buenos Aires deglaciation is entirely consistent with that of other mid-latitude South American records, indicating that the main transition to the present interglacial climate was apparently under way by or ca. 16 ka (Ariztegui et al., 1997; Denton, 1999; Markgraf, 2001).

Global Glacial Signal?

The similarity between the structure of the last mid-latitude South American ice age and that in the Northern Hemisphere is remarkable from the perspective of insolation differences. Despite high insolation, glaciers advanced out of the southern Andes and fluctuated on the Patagonian plains during stage 2, the definition of which reflects the most voluminous and expansive Northern Hemisphere ice sheets and mountain glaciers in the last glacial cycle (Fig. 5; Shackleton et al., 1990). The range of cosmogenic ages (23–16 ka) obtained at Lago Buenos Aires at 46 °S is nearly identical to distribution of cosmogenic ages obtained for the North American Sierra Nevada Tioga glacial advances (23–16 ka; Phillips et al., 1996) and classic Rocky Mountain Pinedale glaciation in the west Wind River (21.8–15.7; Gosse et al., 1995) and east Wind River Range (23–16 ka; Phillips et al., 1997). Moreover, the timing of major deglaciation at Lago Buenos Aires, after ca. 16 ka, along with other paleoclimate proxies in southern South America, suggests that the last glaciation persisted until a similar time in the mid-latitudes of both hemispheres (Ariztegui et al., 1997; Denton, 1999; Licciardi et al., 2001; Markgraf, 2001).

Despite maximum Southern Hemisphere insolation, in many areas the most extensive Patagonian ice extent during stage 2 occurred in phase with the coldest period at GISP2 in the North Atlantic region (e.g., Alley et al., 2002). In fact, the timing of maximum outlet glacier extent on both sides of the Andes, prior to ca. 22 ka, with exceptions ca. 18–17 ka (Denton, 1999), is similar in timing to the two most extensive periods for many portions of the Northern Hemisphere ice sheets and mountain glaciers (e.g., Denton and Hughes, 1981; Phillips et al., 1996, 1997; Licciardi et al., 2001; Dyke et al., 2002). In the Northern Hemisphere, these two glacially extensive periods of stage 2 are reflected in part by Heinrich events 2 and 1 (Denton, 1999); thus, considering all records, there is tantalizing evidence from mid-latitude South America that the most extensive glacial advances also occurred at these times (Fig. 5B).

The glacial geologic record in the Andes from ~36°S to 46°S implies low snowlines from ca. 27 ka to 16 ka (Fig. 5B), which ranged from 0 to 3000 m between ~60° to 30°S (Broecker and Denton, 1989). The correspondence with the timing of snowline depression at equivalent latitudes in the Northern Hemisphere (e.g., Denton and Hughes, 1981; Gosse et al., 1995; Phillips et al., 1996, 1997; Licciardi et al., 2001) suggests that reduced atmospheric temperature was a dominant forcing behind interhemispheric climate change and glacial expansion (Broecker and Denton, 1989). Broecker and Denton (1989) emphasized that an equivalent amount of former snowline depression in both hemispheres suggests global temperature lowering. At the time, however, a lack of chronological constraints in many regions prevented secure knowledge of the age of the mapped snowline depression, which is now well documented in mid-latitude South America using three independent dating approaches (Fig. 5).

Because precipitation can play an important role in glacial behavior, we suspect that it also plays a key part in causing Southern Hemisphere glacier variability. In the southern Andes, precipitation variability is closely linked to the latitudinal fluctuations of the southern Westerlies. Thus, differences in relative ice extent and leads and lags between terrestrial records (Fig. 5B) are to be expected and contain important paleoclimate information, especially on millennial time scales.

To understand the processes that drive glacial climates, the structure of the last glacial

period in southern South America must be considered prominently in addition to ocean and Antarctic ice core records that show differences between the hemispheres during stage 2, including a rapid rise to interglacial sea surface temperatures (Lea, 2001) and isotope values in the Vostok and Byrd ice cores ca. 20 ka (e.g., Blunier et al., 1998; Petit et al., 1999). Relative to the Northern Hemisphere, the South American records preclude any forcing mechanism that would have caused asynchronous hemisphere-wide climate response throughout the ca. 23–16 ka last glacial maximum. This conclusion lends strong support to the proposition of Denton (1999), who pointed out that many facets of the Last Glacial Maximum in the Lake District (Fig. 1), such as the post-17 ka termination, are incompatible with complete asynchrony between the hemispheres, specifically if caused by an ocean-heat forcing or bipolar see-saw mechanism (Stocker, 2000). The challenge now is to accommodate the apparently diverse proxy records from Antarctic ice, marine sediments, and terrestrial South America to generate models that fully simulate Southern Hemisphere ice ages.

CONCLUSIONS

In the area of Lago Buenos Aires, new cosmogenic exposure ages, $^{40}Ar/^{39}Ar$-dated lavas, and the ^{14}C age of varved sediment are remarkably consistent with one another and with the relative ages of the moraines and lava flows. This speaks to both the accuracy and precision of the cosmogenic ages and the excellent capacity that exposure dating holds for elucidating the recent history of Patagonian ice fluctuations. Although our chronology is provisional prior to ca. 25 ka, it appears that there are no stage 4 moraines at Lago Buenos Aires, indicating that any glacial advances during this time extended to or less than the maximum area covered by ice during stage 2, when the Fenix V moraine was deposited ca. 23 ka.

Although Southern Hemisphere insolation was anti-phased with that in the Northern Hemisphere, the structure of the last glaciation at Lago Buenos Aires and in the mid-latitude southern Andes with an overall timing of ca. 23–16 ka, a maximum ice extent prior to ca. 22 ka, and deglaciation after or ca. 16 ka, is nearly identical to that of mid-latitude Rocky and Sierra Mountain glaciers and the Northern Hemisphere ice sheets. In addition, the timing of most extensive ice on the Patagonian plains is coeval with the coldest part of stage 2 recorded at GISP2 in the North Atlantic region (Alley et al., 2002). Changes in Northern Hemisphere insolation were clearly an important pacemaker in the timing of the most recent ice age deep within southern South America. Thus, a climate forcing mechanism such as a relatively rapid fall in atmospheric temperature as Northern Hemisphere insolation decreased must have caused the global stage 2 ice age. A more precise cosmogenic chronology will further resolve low- and high-frequency fluctuations of Patagonian glaciers, thereby documenting the similarities and differences between southern glacial climates and those in the Northern Hemisphere during the last, penultimate, and earlier glaciations.

ACKNOWLEDGMENTS

We thank Marc W. Caffee at Lawrence Livermore National Laboratory for ^{10}Be and ^{26}Al measurements; Brian Beard, Clark Johnson, Jorge Rabassa, Ryan Clark, Alissa Naymark, and Petty and Coco Nauta for laboratory and logistical assistance; Waldmer Keller at the University of Zurich for ^{14}C dating; Fred Luiszer and John Drexler for ICP analyses; and Michael Bentley and Jörg Schäfer for very helpful reviews. This work was supported by National Science Foundation grants EAR-9909309 and ATM-0212450 (Singer), a Weeks Postdoctoral Fellowship (Kaplan), NSF-ATM-980960 (M. Kurz), and the Woods Hole Oceanographic Institution Ventures Fund (R. Ackert).

REFERENCES CITED

Ackert, R.P., Singer, B.S., Guillou, H., Kaplan, M.R., and Kurz, M.D., 2003, Long-term cosmogenic ^{3}He production rates from $^{40}Ar/^{39}Ar$ and K-Ar dated Patagonian lava flows at 47 °S: Earth and Planetary Science Letters, v. 210, p. 119–136.

Alley, R.B., Brook, E.J., and Anandakrishnan, S., 2002, A northern lead in the orbital band: North-south phasing of ice-age events: Quaternary Science Reviews, v. 21, p. 431–441.

Ariztegui, D., Bianchi, M.M., Masaferro, J., Lafargue, E., and Niessen, F., 1997, Interhemispheric synchrony of Late-glacial climatic instability as recorded in proglacial Lake Mascardi, Argentina: Journal of Quaternary Science, v. 12, p. 333–338.

Basile, I., Grousset, F.E., Revel, M., Petit, J.R., Biscaye, P.E., and Barkov, N.I., 1997, Patagonian origin of glacial dust deposited in East Antarctica (Vostok and Dome C) during glacial stages 2, 4, and 6: Earth and Planetary Science Letters, v. 146, p. 573–589.

Beck, J.W., Richards, D.A., Edwards, R.L., Silverman, B.W., Smart, P.L., Donahue, D.J., Hererra-Osterheld, S., Burr, G.S., Calsoyas, L., Jull, A.J.T., and Biddulph, D., 2001, Extremely large variations of atmospheric ^{14}C concentration during the last glacial period: Science, v. 292, p. 2453–2458.

Berger, A., and Loutre, M.F., 1991, Insolation values for the climate of the last 10 million years: Quaternary Science Reviews, v. 10, p. 297–318.

Blunier, T., Chappellaz, J., Schwander, J., Dällenbach, A., Stauffer, B., Stocker, T.F., Raynaud, D., Jouzel, J., Clausen, H.B., Hammer, C.U., and Johnsen, S.J., 1998, Asynchrony of Antarctic and Greenland climate change during the last glacial period: Nature, v. 394, p. 739–743.

Broecker, W.S., and Denton, G.H., 1989, The role of ocean-atmosphere reorganizations in glacial cycles: Geochimica et Cosmochimica Acta, v. 53, p. 2465–2501.

Brown, E.T., Brook, E.J., Raisbeck, G.M., Yiou, F., and Kurz, M.D., 1992, Effective attenuation of cosmic rays producing ^{10}Be and ^{26}Al in Quartz: Implications for exposure dating: Geophysical Research Letters, v. 19, p. 369–372.

Caldenius, C.G., 1932, Las glaciaciones Cuaternarias en la Patagonia and Tierra del Fuego: Geografiska Annaler, v. 14, p. 1–164.

Cane, M., and Clement, A.C., 1999, A role for the tropical Pacific coupled ocean-atmosphere system on Milankovitch and millennial timescales. Part II: Global impacts, *in* Clark, P., Webb, R.S., and Keigwin, L.D., eds., Mechanisms of global climate change at millennial time scales: Washington, D.C., American Geophysical Union, p. 373–383.

Cerling, T.E., 1990, Dating geomorphic surfaces using cosmogenic ^{3}He: Quaternary Research, v. 22, p. 148–156.

Cerling, T.E., and Craig, H., 1994, Geomorphology and in-situ cosmogenic isotopes: Annual Reviews of Earth and Planetary Science, v. 22, p. 273–317.

Clapperton, C.M., 1993, Quaternary geology and geomorphology of South America: New York, Elsevier, 779 p.

Clapperton, C., and Seltzer, G., 2001, Glaciation during marine isotope Stage 2 in the American Cordillera, *in* Markgraf, V., ed., Interhemispheric climate linkages: San Diego, Academic Press, p. 173–181.

Denton, G.H., ed., 1999, Glacial and vegetational history of the southern Lake District of Chile: Geografiska Annaler, 81A, 358 p.

Denton, G.H., and Hughes, T.J., 1981, The last great ice sheets: New York, John Wiley and Sons, 484 p.

Denton, G.H., Heusser, C.J., Lowell, T.V., Moreno, P.I., Andersen, B.G., Heusser, L.E., Schluchter, C., and Marchant, D.R., 1999, Interhemispheric linkage of paleoclimate during the last glaciation: Geografiska Annaler, v. 81, p. 107–153.

Dunai, T.J., 2000, Scaling factors for production rates of in-situ produced cosmogenic nuclides: A critical reevaluation: Earth and Planetary Science Letters, v. 176, p. 157–169.

Dunai, T.J., 2001, Influence of secular variation of the geomagnetic field on production rates of in-situ produced cosmogenic nuclides: Earth and Planetary Science Letters, v. 193, p. 203–218.

Dyke, A.S., Andrews, J.T., Clark, P.U., England, J.H., Miller, G.H., Shaw, J., and Veillette, J.J., 2002, The Laurentide and Innuitian Ice Sheets during the Last Glacial Maximum: Quaternary Science Reviews, v. 21, p. 9–31.

Elliot, M., Labeyrie, L., Bond, G., Cortyo, E., Ruron, J.-L., Tisnerat, N., and Duplessy, J.C., 1998, Millennial-scale iceberg discharges in the Irminger Basin during the last glacial period: Relationship with the Heinrich events and environmental settings: Paleoceanography, v. 13, p. 433–446.

Farley, K.A., Wolf, R.A., and Silver, L.T., 1996, The effects of long alpha-stopping distances on (U-Th)/He dates: Geochimica Cosmochimica Acta, v. 60, p. 4223–4229.

Gosse, J.C., and Phillips, F.M., 2001, Terrestrial in situ cosmogenic nuclides: Theory and application: Quaternary Science Reviews, v. 20, p. 1475–1560.

Gosse, J.C., and Stone, J.O., 2001, Terrestrial cosmogenic nuclide methods passing milestones toward paleoaltimetry: Eos (Transactions, American Geophysical Union), v. 82, p. 82, 86, 89.

Gosse, J.C., Klein, J., Evenson, E.B., Lawn, B., and Middleton, R., 1995, Beryllium-10 dating of the duration and retreat of the last Pinedale glacial sequence: Science, v. 268, p. 1329–1333.

Guyodo, Y., and Valet, J.-P., 1999, Global changes in intensity of the Earth's magnetic field during the past 800 kyr: Nature, v. 399, p. 249–252.

Heusser, C.J., Heusser, L.E., and Lowell, T.V., 1999, Paleoecology of the Southern Chilean Lake District-Isla Grande de Chiloé during middle–late Llanquihue glaciation and deglaciation: Geografiska Annaler, v. 81, p. 231–284.

Kohl, C.P., and Nishiizumi, K., 1992, Chemical isolation of quartz for measurement of in-situ-produced cosmogenic nuclides: Geochimica et Cosmochimica Acta, v. 56, p. 3583–3587.

Krogh, T.E., 1982, Improved accuracy of U-Pb zircon ages by the creation of more concordant systems using an air abrasion technique: Geochimica Cosmochimica Acta, v. 46, p. 637–649.

Kurz, M.D., 1986, In situ production of terrestrial cosmogenic helium and some applications to geochronology: Geochimica Cosmochimica Acta, v. 50, p. 2855–2862.

Kurz, M.D., and Brook, E.J., 1994, Surface exposure dating with cosmogenic nuclides, *in* Beck, C., ed., Dating in exposed and surface contexts: Albuquerque, University of New Mexico Press, p. 139–159.

Kurz, M.D., Colodner, D., Trull, T.W., Moore, R.B., and O'Brien, K., 1990, Cosmic ray exposure dating with in-situ produced cosmogenic ^{3}He: Results from young Hawaiian lava flows: Earth and Planetary Science Letters, v. 97, p. 177–189.

Kurtz, M.D., Kenna, T.C., Lassiter, J.C., and DePaolo, D.J., 1996, Helium isotopic evolution of Mauna Kea Volcano: First results from the 1 km drill core: Journal of Geophysical Research, v. 101, p. 11,781–11,791.

Lal, D., 1991, Cosmic ray labeling of erosion surfaces: In-situ nuclide production rates and erosion models: Earth and Planetary Science Letters, v. 104, p. 424–439.

Lea, D.W., 2001, Ice ages, the California Current, and Devils Hole: Science, v. 293, p. 59–60.

Licciardi, J.M., Kurz, M.D., Clark, P.U., and Brook, E.J., 1999, Calibration of cosmogenic ^{3}He production rates from Holocene lava flows in Oregon, USA, and effects of the Earth's magnetic field: Earth and Planetary Science Letters, v. 172, p. 261–271.

Licciardi, J.M., Clark, P.U., Brook, E.J., Pierce, K.L., Kurz, M.D., Elmore, D., and Pankaj, S., 2001, Cosmogenic ^{3}He and ^{10}Be chronologies of the late Pinedale northern Yellowstone ice cap, Montana, USA: Geology, v. 29, p. 1095–1098.

Markgraf, V., ed., 2001, Interhemispheric climate linkages: San Diego, Academic Press, 454 p.

Masarik, J., Frank, M., Schäffer, J.M., and Wieller, R., 2001, Correction of in situ cosmogenic nuclide production rates for geomagnetic field intensity variations during the past 800,000 years: Geochimica et Cosmochimica Acta, v. 65, p. 2995–3003.

McElhinny, M.W., and Senanayake, W.E., 1982, Variations in the geomagnetic dipole 1: The past 50,000 years: Journal of Geomagnetism and Geoelectricity, v. 34, p. 39–51.

Mercer, J.H., 1969, Glaciation in southern Argentina more than two million years ago: Science, v. 164, p. 823–825.

Mercer, J.H., 1976, Glacial history of southernmost South America: Quaternary Research, v. 6, p. 125–166.

Mercer, J.H., 1983, Cenozoic glaciation in the Southern Hemisphere: Annual Reviews of Earth and Planetary Science, v. 11, p. 99–132.

Mörner, N.-A., and Sylwan, C., 1989, Magnetostratigraphy of the Patagonian moraine sequence at Lago Buenos Aires: Journal of South American Earth Sciences, v. 2, p. 385–389.

Nishiizumi, K., Winterer, E.L., Kohl, C.P., Klein, J., Middleton, R., Lal, D., and Arnold, J.R., 1989, Cosmic ray production rates of ^{10}Be and ^{26}Al in quartz from glacially polished rocks: Journal of Geophysical Research, v. 94, p. 17907–17915.

Ohno, M., and Hamano, Y., 1992, Geomagnetic poles over the last 10,000 years: Geophysical Research Letters, v. 19, p. 1715–1718.

Ohno, M., and Hamano, Y., 1993, Global analysis of the geomagnetic field: Time variation of the dipole moment and the geomagnetic pole in the Holocene: Journal of Geomagnetism, Geoelectricity, v. 45, p. 1455–1466.

Petit, J.R., Jouzel, J., Raynaud, D., Barkov, N.I., Barnola, J.M., Basile, I., Bender, M., Chappellaz, J., Davis, M., Delaygue, G., Delmotte, M., Kotlyakov, V.M., Legrand, M., Lipenkov, V.Y., Lorius, C., Pépin, L., Ritz, C., Saltzmank, E., and Stievenard, M., 1999, Climate and atmospheric history of the past 420,000 years from the Vostok ice core, Antarctica: Nature, v. 399, p. 429–436.

Phillips, F.M., Zreda, M.G., Plummer, M.A., Benson, L.V., Elmore, D., and Sharma, P., 1996, Chronology for fluctuations in Late Pleistocene Sierra Nevada glaciers and lakes: Science, v. 274, p. 749–751.

Phillips, F.M., Zreda, M.G., Gosse, J.C., Klein, J., Evenson, E.B., Hall, R.D., Chadwick, O.A., and Sharma, P., 1997, Cosmogenic ^{36}Cl and ^{10}Be ages of Quaternary glacial and fluvial deposits of the Wind River Range, Wyoming: Geological Society of America Bulletin, v. 109, p. 1453–1463.

Rabassa, J., and Clapperton, C.M., 1990, Quaternary glaciations in the southern Andes: Quaternary Science Reviews, v. 9, p. 153–174.

Shackleton, N.J., Berger, A., and Peltier, W.R., 1990, An alternative astronomical calibration of the lower Pleistocene timescale based on ODP site 677: Transactions of the Royal Society of Edinburgh, Earth Sciences, v. 81, p. 251–261.

Singer, B.S., Thompson, R.A., Dungan, M.A., Feeley, T.C., Nelson, S.T., Pickens, J.C., Brown, L.L., Wulff, A.W., Davidson, J.P., and Metzger, J., 1997, Volcanism and erosion during the past 930 thousand years at the Tatara–San Pedro complex, Chilean Andes: Geological Society of America Bulletin, v. 109, p. 127–142.

Singer, B., Hildreth, W., and Vincze, Y., 2000, ^{40}Ar/^{39}Ar evidence for early deglaciation of the central Chilean Andes: Geophysical Research Letters, v. 27, p. 1663–1666.

Singer, B.S., Ackert, R.P., and Guillou, H., 2004, ^{40}Ar/^{39}Ar and K-Ar chronology of Pleistocene glaciations in Patagonia: Geological Society of America Bulletin, v. 116, no. 3/4, p. 434–450.

Small, E.E., Anderson, R.S., Repka, J.R., and Finkel, R., 1997, Erosion rates of alpine bedrock summit surfaces deduced from in situ ^{10}Be and ^{26}Al: Earth and Planetary Science Letters, v. 150, p. 413–425.

Steig, E.J., Brook, E.J., White, J.W., Sucher, C.M., Bender, M.L., Lehman, S.J., Morse, D.L., Waddington, E.D., and Clow, G.D., 1998, Synchronous climate changes in Antarctica and the north Atlantic: Science, v. 282, p. 92–95.

Stocker, T.F., 2000, Past and future reorganizations in the climate system: Quaternary Science Reviews, v. 19, p. 301–319.

Stone, J.O., 2000, Air pressure and cosmogenic isotope production: Journal of Geophysical Research, v. 105, p. 23,753–23,759.

Stuiver, M., Reimer, P.J., Bard, E., Beck, J.W., Burr, G.S., Hughen, K.A., Kromer, B., McCormack, F.G., van der Plicht, J., and Spurk, M., 1998, INTCAL98 Radiocarbon age calibration 24,000–0 cal BP: Radiocarbon, v. 40, p. 1041–1043.

Sylwan, C.A., 1989, Paleomagnetism, paleoclimate, and chronology of Late Cenozoic deposits in southern Argentina [Ph.D. thesis]: Sweden, Stockholm University, 110 p.

Taljaard, J.J., van Loon, H., Cructcher, H.L., and Jenne, R.L., 1969, Climate of the upper air: Southern Hemisphere, Vol. 1, temperatures, dew points, and heights at selected levels NAVAIR 50–1C–55: Washington D.C., Chief Naval Operations, Naval Weather Service Command.

Taylor, J.R., 1982, An introduction to error analysis: Mill Valley, California, University Science Books, 270 p.

Ton-That, T., Singer, B., Mörner, N., and Rabassa, J., 1999, Datación por el método ^{40}Ar/^{39}Ar de lavas basalticas y geología del Cenozoico superior en la región del Lago Buenos Aires, provincia de Santa Cruz, Argentina: Revista de la Asociación Geológica Argentina, v. 54, p. 333–352.

Zreda, M.G., Phillips, F.M., Elmore, D., Kubik, P.W., Sharma-Pankaj, and Dorn, R.I., 1991, Cosmogenic chlorine-36 production rates in terrestrial rocks: Earth and Planetary Science Letters, v. 105, p. 94–109.

MANUSCRIPT RECEIVED BY THE SOCIETY 13 MAY 2002
REVISED MANUSCRIPT RECEIVED 23 MAY 2003
MANUSCRIPT ACCEPTED 23 JUNE 2003

Printed in the USA